Annales
Geophysicae

Dust sputtering within the inner heliosphere: a modelling study

Carsten Baumann[1,2]**, Margaretha Myrvang**[1]**, and Ingrid Mann**[1]

[1]UiT The Arctic University of Norway, Space Physics Group, Postboks 6050 Langnes, 9037 Tromsø, Norway
[2]Deutsches Zentrum für Luft- und Raumfahrt, Institut für Solar-Terrestrische Physik, Neustrelitz, Germany

Correspondence: Carsten Baumann (carsten.baumann@dlr.de)

Abstract. The aim of this study is to investigate through modelling how sputtering by impacting solar wind ions influences the lifetime of dust particles in the inner heliosphere near the Sun.

We consider three typical dust materials, silicate, $Fe_{0.4}Mg_{0.6}O$, and carbon, and describe their sputtering yields based on atomic yields given by the Stopping and Range of Ions in Matter (SRIM) package. The influence of the solar wind is characterized by plasma density, solar wind speed, and solar wind composition, and we assume for these parameter values that are typical for fast solar wind, slow solar wind, and coronal mass ejection (CME) conditions to calculate the sputtering lifetimes of dust. To compare the sputtering lifetimes to typical sublimation lifetimes, we use temperature estimates based on Mie calculations and material vapour pressure derived with the MAGMA chemical equilibrium code. We also compare the sputtering lifetimes to the Poynting–Robertson lifetime and to the collision lifetime.

We present a set of sputtering rates and lifetimes that can be used for estimating dust destruction in the fast and slow solar wind and during CME conditions. Our results can be applied to solid particles of a few nanometres and larger. The sputtering lifetimes increase linearly with the size of particles. We show that sputtering rates increase during CME conditions, primarily because of the high number densities of heavy ions in the CME plasma. The shortest sputtering lifetimes we find are for silicate, followed by $Fe_{0.4}Mg_{0.6}O$ and carbon. In a comparison between sputtering and sublimation lifetimes we concentrate on the nanodust population. The comparison shows that sublimation is the faster destruction process within 0.1 AU for $Fe_{0.4}Mg_{0.6}O$, within 0.05 AU for carbon dust, and within 0.07 AU for silicate dust. The destruction by sputtering can play a role in the vicinity of
the Sun. We discuss our findings in the context of recent F-corona intensity measurements onboard Parker Solar Probe.

1 Introduction

New observations onboard Parker Solar Probe (PSP) raised interest again in the dust destruction in the vicinity of the Sun. The corona observations with the Wide-Field Imager for Solar Probe (WISPR) (Howard et al., 2019) onboard PSP include the F corona that is produced by circumsolar dust. The observed corona intensity decreases with decreasing PSP distance from the Sun, and this slope changes at 17 solar radii; dust depletion is mentioned as one of the possible explanations for this observation (Howard et al., 2019). While it seems established that a dust-free zone around the Sun forms because of dust sublimation, model calculations predict that for most materials the dust-free zone would be within 15 solar radii, often even within 10 solar radii (Mann et al., 2004). For dust destruction at larger distances, the sputtering process becomes important.

Parker Solar Probe (Fox et al., 2016) and Solar Orbiter (Müller et al., 2013) will help to quantify the dust component in the inner heliosphere with unprecedented detail. These spacecraft do not carry dedicated dust sensors but can measure the dust component from the F-corona intensity as mentioned above and detect high-velocity dust impacts on the satellite body using electric field sensors. The dust impacts are observed because they change the floating potential of the spacecraft for short periods of time (see e.g. Zaslavsky, 2015).

The FIELDS instrument (Bale et al., 2016) detects dust impacts on the PSP spacecraft. The expected signals due to dust impacts in the vicinity of the Sun were recently

considered based on the results of previous space observations and laboratory studies (Mann et al., 2019). Analysis of FIELDS observations during the three first perihelion passages suggests that the dust density within about 50 solar radii varies by about 50 % between the different encounters (David Malaspina, personal communication, 2020). Dust destruction by sputtering is an efficient process within 50 solar radii and, because the sputtering rates depend on the solar wind conditions, it can vary with time. In addition, Szalay et al. (2020) report the first interpretations of the PSP dust impact data. They explain the measured impact count rate as µm sized dust flux of β-meteoroid type. Since the signals that are observed are due to the charge production during dust impacts, there is no direct information on the size of dust particles. Other space missions also observe nanometre-sized dust (e.g. Meyer-Vernet et al., 2009a, b).

Sputtering, i.e. the emission of atoms from a surface due to the impact of energetic ions, occurs within the whole heliosphere as solar wind ions hit dust particles. Sublimation of dust, i.e. the phase transition of a body due to absorption of solar radiation and subsequent increase in its vapour pressure, happens only when the equilibrium temperature exceeds the binding energy of the atoms in the dust structure.

Within the heliosphere, solar radiation and energetic particles are intensive enough to form thin abrasive exospheres as at Mercury (e.g. McGrath et al., 1986; Wurz, 2012) or moons (e.g. Wurz et al., 2007; Killen et al., 2012; Vorburger et al., 2019). Dust in the heliosphere outside of 1 AU is more affected by sputtering; examples are the dust on the surface of comet 67P/Churyumov-Gerasimenko (Wurz et al., 2015) or ice grains in Saturn's magnetosphere (Johnson et al., 2008).

Theoretical considerations suggest that the nanodust is trapped under certain conditions in orbits around the Sun (Czechowski and Mann, 2010; Stamm et al., 2019). While the trajectories of dust particles are influenced by the bombardment of solar energetic ions (Ragot and Kahler, 2003), our work concentrates on the survival of nanodust during passages of coronal mass ejections (CMEs) and the solar wind. Czechowski and Kleimann (2017) carried out dust trajectory calculations within a CME scenario and found trapped as well as ejected nanodust trajectories. However, the vast amount of energetic plasma ejected during a CME does not leave the nanodust untouched. We investigate dust destruction by sputtering and consider the conditions near the Sun, for which this process becomes important in comparison to the sublimation of dust particles.

This study is organized as follows: Sect. 2 introduces the solar wind and CME composition as well as plasma densities used in this study. This section also covers the sputtering process of dust within our solar system. Section 3 investigates the sublimation process for dust approaching the vicinity of the Sun. The comparison of both dust loss processes and its implication for dust near the Sun is described within Sect. 4. Finally, Sect. 5 draws the conclusions of this study.
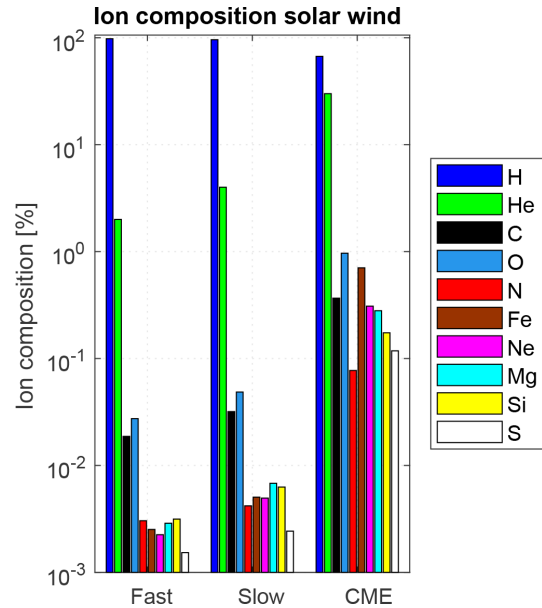

Figure 1. Mean composition of the fast and slow solar wind and CMEs (data taken from Killen et al., 2012).

2 Dust sputtering

Sputtering is the physical process of atom ejection from a solid through the bombardment of energetic ions (Behrisch and Eckstein, 2007). This process usually is performed within a laboratory environment where a cathode is bombarded with noble gas ions and the ejected cathode atom deposits and forms high-quality surfaces (see Greene, 2017, for a review). However, this process is also well known in the context of dust destruction for interplanetary (e.g. Mukai and Schwehm, 1981) and interstellar dust grains (e.g. Barlow, 1978; Draine and Salpeter, 1979).

For the calculation of nanodust sputtering, we divide our study into three different sputtering scenarios. These are the slow solar wind conditions, fast solar wind conditions, and CME conditions. In the following, the heliospheric conditions of these scenarios are discussed in detail. Subsequently, we introduce the calculation of the dust's sputtering lifetimes. This is followed by an analysis of dust sputtering at 1 AU and in the inner heliosphere.

2.1 Heliospheric conditions

Figure 1 shows the composition of the three solar wind scenarios considered. The solar wind and CME compositions used here are based on the work of Killen et al. (2012, their Table 6) and contain 10 different species, including protons (H), helium ions (He), and the heavier species carbon (C), oxygen (O), nitrogen (N), iron (Fe), neon (Ne), magnesium (Mg), silicon (Si), and sulfur (S) ions. Generally, the solar wind is composed of a big fraction of protons, a small fraction of helium, and traces of the heavier species. The com-

position changes between 96 % H/4 % He for the slow solar wind and 98 % H/2 % He for the fast solar wind, with heavier species around 0.1 %. The composition of CMEs however is much more dominated by heavier species, 67 % H 30 % He, and 3 % heavier species. In addition to the plasma composition, the plasma speed and density are also different for each solar wind scenario. Table 1 summarizes the values that have been used for the solar wind as well as CME conditions within this study. It has to be noted that the composition, speed, and plasma density of the solar wind or CMEs are highly variable. The given values describe average conditions.

Sputtering is the impact process of an energetic ion or atom on a target and the subsequent removal of target atoms from its surface. The sputtering yield is the main parameter of the sputtering process itself. This yield denotes the number of target atoms sputtered by one incident ion and is a function of the ion's kinetic energy and the target's material properties (e.g. Behrisch and Eckstein, 2007, and references therein).

For further analysis we have retrieved the sputtering yield for carbon, $Fe_{0.4}Mg_{0.6}O$, and astronomical silicate ($MgFeSiO_4$) hit by nine different solar wind (SW) ions. For the $Fe_{0.4}Mg_{0.6}O$ and silicate we have used the SRIM (Stopping and Range of Ions in Matter) package (Ziegler et al., 2008) that derives the sputtering yields and also stopping powers and ranges of ions within compounds. For each solar wind scenario, the SRIM program has been initialized by the above-mentioned plasma composition and speed (energy/nucleii). In order to derive the sputtering yield for the dust species i for a given scenario, we summed up the sputtering yields for each atom j sputtered by solar wind ion k.

$$Y_i = \sum_{j,k} Y_{i,j,k} \tag{1}$$

The index j denotes the target atoms Mg/Fe/Si/O for astronomical silicate and Fe/Mg/O for the $Fe_{0.4}Mg_{0.6}O$ composition. The yields correspond to the atomic abundance ratios of the dust composition and the ion ratio of the solar wind composition. For the mono-atomic carbon case we have used the analytic formula from Eckstein and Preuss (2003) together with the experimentally fitted sputtering parameters (Behrisch and Eckstein, 2007, and references cited within pages 45–46). The result of these calculations are sputtering yields for silicate, $Fe_{0.4}Mg_{0.6}O$, and carbon for the three different sputtering scenarios, i.e. slow SW/fast SW/CME. The individually derived yields can be found in the Supplement.

Figure 2 shows the results of the assessment, i.e. the sputtering yield as a function of ion species (H – sulfur S), for the three different materials. The given values are not absolute but prorated with solar wind ion composition present in fast and slow solar wind as well as CME conditions ($Y_{i,k} \cdot c_k$; c_k is the fractional abundance of ion k in the solar wind conditions; cf. Eq. 1, Table 1). The highest sputtering yields are found for $Fe_{0.4}Mg_{0.6}O$ material; the yields are somewhat
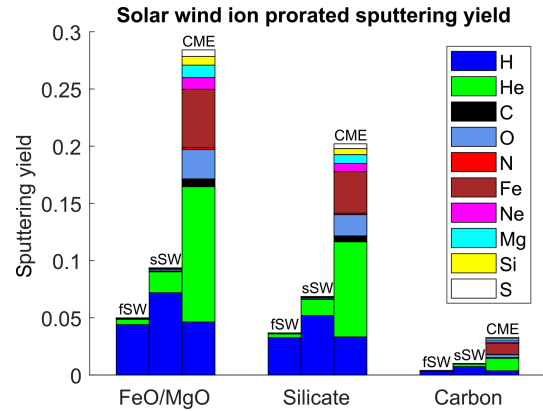
Figure 2. Solar wind ion prorated sputtering yield for $Fe_{0.4}Mg_{0.6}O$, silicate, and carbon. Sputtering yields are a function of solar wind ion itself, its fractional abundance (fast solar wind (fSW), slow solar wind (sSW), and CME), and its mean speed.

smaller for silicate and are the lowest by far for carbon material. Figure 2 also shows that the sputtering yields strongly increase during CME conditions and that this is due to the sputtering by the heavy ions that are more abundant during CME than in the normal solar wind. Likewise, the higher abundance of He ions in the slow solar wind explains why sputtering yields are larger in the slow solar wind than in the fast solar wind.

The sputtering yields for carbon are significantly lower than for the silicate and $Fe_{0.4}Mg_{0.6}O$ materials. In addition, Fig. 2 shows the strong enhancement of the sputtering yield in the case of CME conditions due to the higher abundance of heavier ion species. The higher abundance of He ions in the slow solar wind conditions is the reason for the higher sputtering yields compared to the fast solar wind. This is the case for all three dust components.

Absolute sputtering yields are listed in the Supplement. They depend on the target material and strongly vary with the mass of the sputtering ion. The yields for sputtering by iron ions are for instance 2 orders of magnitude higher than those for sputtering by protons, and this is so for all the target materials. Comparing the sputtering yields for the three different ion speeds considered, those for $300\,km\,s^{-1}$ are the highest, those for $500\,km\,s^{-1}$ are 20 % lower, and those for $800\,km\,s^{-1}$ are 40 % lower.

To show the importance of heavy ion sputtering, especially during CME conditions, we have calculated the relative sputtering yield Yr_k weighed with the plasma composition as follows:

$$Yr_k = \frac{c_k \cdot Y_k}{\sum c_k \cdot Y_k}. \tag{2}$$

c_k denotes the composition of the solar wind plasma as shown in Fig. 1. The weighted sputtering yield for the carbon target material is shown in Fig. 3, and the other target materials show similar results. One can see that the increase

Table 1. Solar wind properties as used within this study. Helium and heavy ion fractions of the solar wind are used from Killen et al. (2012).

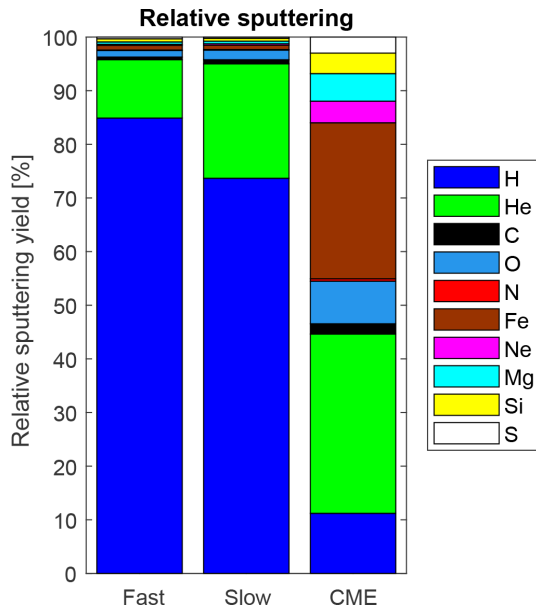|	Plasma density n_p	Speed v_p	He fraction	Heavy ion frac.
Slow SW	$8\,\mathrm{cm}^{-3}$	$300\,\mathrm{km\,s}^{-1}$	4 %	0.11 %
Fast SW	$3\,\mathrm{cm}^{-3}$	$800\,\mathrm{km\,s}^{-1}$	2 %	0.06 %
CME	$70\,\mathrm{cm}^{-3}$	$500\,\mathrm{km\,s}^{-1}$	30 %	3 %

Figure 3. Weighed relative sputtering yield of carbon for the three different solar wind compositions; results for astronomical silicate and $Fe_{0.4}Mg_{0.6}O$ are similar, but the absolute values vary according to Fig. 2.

in heavy ions in CME, which is small in numbers, results in a much higher contribution of these ions to the sputtering yield; in turn we expect that this strongly influences sputtering efficiencies. Other works on sputtering have considered H and He as components of the fast and slow SW (e.g. Wurz et al., 2010) only. This is a valid simplification for general solar wind conditions. Our calculation shows that considering heavy ions barely influences the sputtering efficiency in the fast and slow SW.

The sputtering yields used in this study have only been derived by considering a normal impact of an ion onto the target particle and a resulting collision cascade governed by atomic forces within the target lattice. However, it has to be noted that the sputtering process is also heavily influenced by a number of additional parameters, which cannot be accounted for in this study. Eventual sputtering yield enhancement can occur due to high target temperatures (Roth and Möller, 1985), non-normal impact angle, ion charge state for sputtering of insulators (Hayderer et al., 2001), and a size dependence of the yield when considering nanometre-sized dust (Järvi et al., 2008). All these processes might enhance

the sputtering yield substantially. On the other hand, microscopic surface roughness can increase but also decrease the sputtering yield under certain circumstances, e.g. slant sputtering (Ruzic, 1990). In addition, we also do not consider composition change due to eventual implementation of solar wind ions into the dust or fractional depletion of a certain atom type within the dust. Due to a lack of quantitative information on these enhancement factors for our study, we use the conservative sputtering yields given by SRIM. As a consequence, our results provide an upper limit for dust sputtering lifetimes. We speculate that dust sputtering lifetimes could be 1 order of magnitude shorter when taking the microphysics of dust sputtering into account.

2.2 Sputtering lifetimes

For the derivation of nanodust sputtering lifetimes, we follow the formalism given by Wurz (2012). The mass loss rate from a surface through sputtering in the solar wind is given by the following:

$$\frac{dm_{\mathrm{sput}}}{dt} = -f_{\mathrm{SW}}Y_{\mathrm{tot}}Am_{\mathrm{A}}. \tag{3}$$

Here, A is the cross section of the dust, f_{SW} the solar wind ion flux, Y_{tot} is the total sputtering yield of the target material, and m_{A} is the mean mass of the sputtered atoms.

Under the assumption of constant composition and size-independent sputtering yield, the sputtering lifetime can be integrated from the sputtering mass loss rate of a circular surface exposed to the SW/CME plasma:

$$t_{\mathrm{sput}} = \frac{4r_0 N_{\mathrm{A}}\rho}{f_{\mathrm{SW}}Y_{\mathrm{tot}}M}. \tag{4}$$

Here, r_0 is the initial radius of the dust, N_{A} is the Avogadro constant, and M and ρ are the molar mass and mass density of the sputtered material. For the solar wind flux $f_{\mathrm{SW}} = n_p \cdot v_p$ the values from Table 1 have been used.

Figure 4 shows sputtering lifetimes of 1 nm dust at a distance of 1 AU from the Sun. Lifetimes for all three plasma conditions and the three different dust compositions are shown.

One can see that carbon nanodust survives longest among all three studied compositions; i.e. 1 nm dust survives 5000 d at 1 AU under CME conditions. $Fe_{0.4}Mg_{0.6}O$ sputtering lifetimes are a factor of 20 shorter. The lifetimes of silicate are a factor of 60 shorter than the carbon sputtering lifetimes.

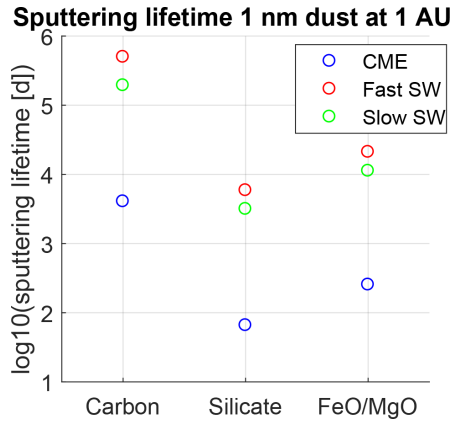**Figure 4.** Sputtering lifetimes for carbon, silicate, and $Fe_{0.4}Mg_{0.6}O$ dust particles at 1 AU and size 1 nm; colour indicates solar wind/CME composition and flux.

Figure 5. Sputtering lifetimes for carbon (dashed), silicate (solid), and $Fe_{0.4}Mg_{0.6}O$ (dotted) dust particles at 1 AU for different sizes; line colour indicates plasma environment (blue – CME conditions, green – slow solar wind, red – fast solar wind). Collisional lifetime (τ_C) and Poynting–Robertson lifetime (τ_{PR}) are shown in black for comparison (data taken from Grün et al., 1985).

These factors vary slightly with all solar wind conditions. When comparing the different solar wind conditions, CME sputtering lifetimes are the shortest. Sputtering lifetimes in the slow solar wind are 20-fold longer. The lifetimes for fast solar wind conditions are 20 times longer than the lifetimes in CME conditions. This behaviour varies a bit from one dust composition to the other. The short lifetimes in the CME scenario occur due to the presence of heavy ions in an overall denser plasma cloud. However, CMEs are distinct solar eruptions, and these sputtering conditions do not last longer than 1 or 2 d and occur only locally in the heliosphere. The given lifetimes of several tens of days and more at 1 AU for 1 nm dust make full destruction due to CME sputtering impossible. However, for the case of fast and slow SW, which is present within the heliosphere at all times, the sputtering lifetimes are close to 10 years in the case of silicate nanodust and 30 years for $Fe_{0.4}Mg_{0.6}O$ nanodust.

The sputtering lifetime described in Eq. (4) is linear in initial dust particle radius and enables easy calculation of lifetimes for other dust sizes. In Fig. 5 we show the derived lifetimes of dust particles in the size range from 1 nm to 1 µm at the Earth's orbit.

Sub-micron dust particles at Earth's orbit have sputtering lifetimes that can reach several hundred thousands of days, i.e. thousands of orbital periods. For a better comparison, the sputtering lifetimes are plotted together with the collisional and Poynting–Robertson lifetimes given by Grün et al. (1985). As mentioned above, only nanodust in the small size limit can be significantly removed by solar wind sputtering in reasonable timescales. For slow and fast solar wind conditions at 1 AU, we find that the sputtering lifetime of silicate particles smaller than 60 nm is clearly below their Poynting–Robertson and collision lifetime. That is also the case for $Fe_{0.4}Mg_{0.6}O$ dust below 30 nm and carbon dust below 20 nm. We point out that for CME conditions at 1 AU we also find that the sputtering lifetime of silicate and $Fe_{0.4}Mg_{0.6}O$ parti-

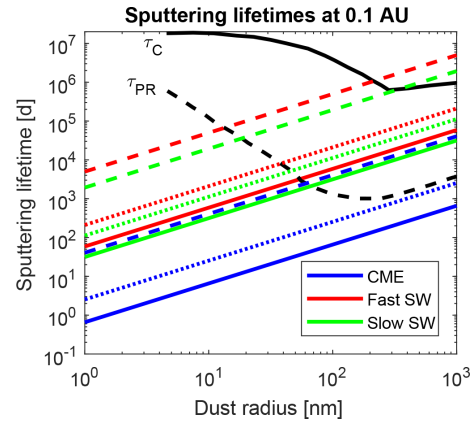cles is well below the Poynting–Robertson and collision lifetime of the dust in the whole considered size interval of 1 to 1000 nm. In practice, this has no consequence because of the short time duration of CMEs. This situation changes when considering sputtering at shorter distances from the Sun, as the SW and CME plasma density increases.

For this approach we consider a SW plasma density following a power law with exponent −2:

$$f_{SW}(d) = f_{SW}(1\,AU)d^{-2}. \tag{5}$$

Here, the distance from the Sun d is given in astronomical units. The used exponent lies within the range of published values; e.g. Maksimovic et al. (2005) report a value of -2.2 ± 0.1. This value was found for the fast SW conditions which we are going to apply for the slow SW and CME conditions as well. Figure 6 shows the lifetime of 1 nm dust at distances from the Sun from 0.01 to 1 AU, derived for the three different SW scenarios and three dust materials. The high vulnerability of silicate to sputtering is visible here too as their solar wind sputtering lifetimes are in the range of the carbon's lifetimes for CME conditions.

As stated above, carbon is a very resistant material with respect to sputtering. Carbon dust with only 1 nm can survive several 10 d at 0.1 AU. Only in the case of sputtering within the CME conditions are the carbon sputtering lifetimes below the typical duration of a CME of 1–2 d within the shortest distances from the Sun.

From the mass loss rate (Eq. 3) it is also possible to derive the erosion rate of a dust particle due to sputtering. This erosion rate, i.e. the shrinkage of dust per unit time (dr / dt), is also independent of dust size.

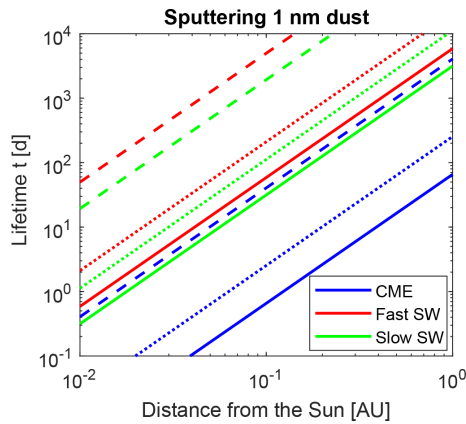$$\frac{dr}{dt}(d) = -\frac{f_{SW}(d)M}{4N_A\rho} \tag{6}$$

Figure 6. Sputtering lifetimes for 1 nm dust for the three different solar wind conditions (blue – CME conditions, red – fast solar wind, green – slow solar wind) as a function of distance from the Sun; line styles indicate the dust compositions ($Fe_{0.4}Mg_{0.6}O$ – dotted, silicate – solid, carbon – dashed).

Table 2. Dust erosion rate for the three compositions and solar wind conditions. Rates are given for 0.1 AU, and the erosion rate is independent of dust size and decreases quadratically with distance from the Sun.

Erosion rate ($nm\,d^{-1}$)	$Fe_{0.4}Mg_{0.6}O$	Silicate	Carbon
Fast SW conditions	5.0×10^{-3}	1.8×10^{-2}	2.1×10^{-4}
Slow SW conditions	9.3×10^{-3}	3.3×10^{-2}	5.4×10^{-4}
CME conditions	0.41	1.6	2.6×10^{-2}

For a distance of 0.1 AU, we derived the erosion rates of the three dust components for the three solar wind conditions in Table 2.

As the dust erosion rate (Eq. 6) is independent of initial dust radius, the sputtering of dust larger than 1 µm can also be considered. For example, a silicate dust particle with a size of 10 µm has a 10 000-fold lifetime of a 1 nm dust grain. When assuming the dust is at a distance of 0.1 AU, the 1 nm dust survives 0.6 d under CME conditions; i.e. it will be destroyed by a single CME. A dust grain of 10 µm size has a lifetime of 6000 d under CME conditions. That means this can be hit by 3000 strong CMEs at a distance of 0.1 AU until it will be finally destroyed. Within our solar system, CME rates vary during a solar cycle. The rate can peak up to 400 per month during high solar activity and can be as low as 10 CMEs per month during solar minimum (Lamy et al., 2019). When assuming a mean value of 100 CMEs per month, the duration a 10 µm particle can survive at 0.1 AU is at least 2.5 years. It has to be noted that this requires that the dust particle is hit by every CME ejected by the Sun. This seems to be unlikely due to the randomness of the CME propagation and its allocated size within the heliosphere. Another reason why the lifetime of bigger dust particles might be unrealistic is that during this period the dust size and its orbit change drasti-
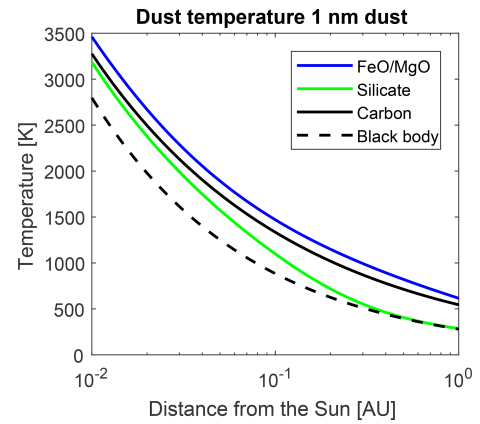

Figure 7. Temperature of 1 nm dust particles as a function of distance; line colour indicates dust composition.

cally. This leads to a different sputtering environment, and the assumption of a constant erosion rate breaks down.

As dust particles approach the vicinity of the Sun, their temperature increases drastically. To investigate the relevance of the sputtering process, the seemingly low nanodust sputtering lifetimes have to be compared to dust destruction by sublimation into free space.

3 Dust sublimation

The processes of sublimation, evaporation, and condensation are usually described by Langmuir's equation of evaporation:

$$\frac{dm_{sub}}{dt} = -p_v \sqrt{\frac{M}{2\pi RT}} A. \tag{7}$$

In case of sublimation, it describes the sublimated mass per time unit as a function of vapour pressure p_v and temperature T of the sublimating material. A is the whole surface of the dust and R is the gas constant. In the context of free space, atoms leave the material's surface into the vacuum, while the adsorption of atoms onto surfaces can also occur under certain conditions, e.g. the resupply of Saturn E rings by the adsorption of Enceladus water vapour (e.g. Hansen et al., 2006). The sublimation of dust particles has been studied within different astrophysical contexts, e.g. protoplanetary systems (e.g. Duschl et al., 1996) and interstellar dust (e.g. Draine and Salpeter, 1979). For a self-consistent study, the sublimation of the same dust materials as in the sputtering part will be considered. In order to quantify the dust sublimation, two parameters are needed, i.e. dust temperature at certain distances from the Sun and the dust materials' vapour pressure.

To derive the dust temperature, we assume the equilibrium of absorbed solar radiation and emitted thermal radiation of the dust particle (Myrvang, 2018). The effect of dust cooling due to evaporation has been quantified to be only 10 % of the emitted power (e.g. Schwehm, 1980), which we neglect in this study. Figure 7 shows the temperature of 1 nm dust particles made of carbon, silicate, and $Fe_{0.4}Mg_{0.6}O$; for comparison, the temperature of a black body is also shown. All nanodust is significantly hotter than a black body, except for silicate near 1 AU, which has similar equilibrium temperatures. Near the Sun, the dust temperatures of all materials exceed the black body. At 0.01 AU the $Fe_{0.4}Mg_{0.6}O$ 1 nm dust is ≈ 700 K hotter than a black body, carbon 500 K, and silicate 400 K. All three materials with a dust size of 1 nm are hotter than 3000 K near the Sun. The temperature change from 1 to 100 nm is below 100 K for each dust material (not shown). These temperatures have been derived using Mie theory, and the refractive indices for carbon and astronomical silicate come from Li and Greenberg (1997). The refractive index for FeO/MgO is from Henning et al. (1995); we have used the data for the $Mg_{0.6}Fe_{0.4}O$ compound.

The second quantity for the description of sublimation is the vapour pressure. For the derivation of the vapour pressure for the oxides $Fe_{0.4}Mg_{0.6}O$ and astronomical silicate, we used the MAGMA code (Fegley and Cameron, 1987; Schaefer and Fegley, 2004). The program is very flexible with regard to material composition and the derived vapour pressures have been checked with a vast number of experimental data. The MAGMA code has been used mainly for the change in planets and planetesimals due to geological activity, but also for the evaporation of meteoroids within the Earth's atmosphere (e.g. Schult et al., 2015). The MAGMA model is a multicomponent gas-melt chemical equilibrium code and is able to derive vapour pressures for mixtures of its base components (MgO, SiO_2, FeO, CaO, Al_2O_3, Na_2O, TiO_2, K_2O, ThO_2, UO_2, PuO_2). The results of the MAGMA model have been successfully compared to experimental work on the vaporization of chondrite-type material. The good performance of the MAGMA model encouraged us to use it in the context of dust sublimation near the Sun as well. The vapour pressure for carbon was used from the literature (Leider et al., 1973; Lide, 2003). Figure 8 (blue lines and left y axis) shows the vapour pressure of all three materials in the temperature range between 500 and 3000 K. The exponential growth of the vapour pressure with temperature is a typical behaviour of all materials. Please pay attention to the comparably low vapour pressure of carbon compared to the oxides: this will have an impact on the dust lifetime.

To derive the sublimation lifetime of nanometre-sized dust particles, Eq. (7) is integrated using spherical geometry (Lamy, 1974):

$$t_{sub}(d, r_0) = \frac{r_0 \rho}{p_v(T_{dust}(d))} \sqrt{\frac{2\pi R T_{dust}(d)}{M}}. \tag{8}$$
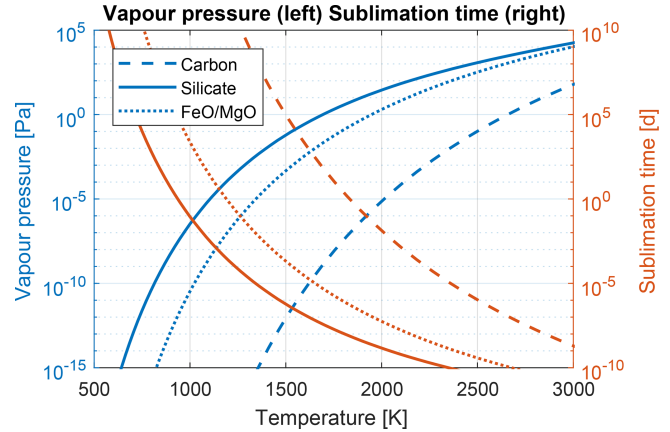

Figure 8. Vapour pressure (blue) and corresponding sublimation lifetime (orange) as a function of 1 nm dust temperature; line styles indicate dust composition (carbon – dashed, astronomical silicate – solid, $Fe_{0.4}Mg_{0.6}O$ – dotted).

Sublimation lifetime

Where p_v is the vapour pressure of the dust material, T_{dust} is the temperature of the nanodust as a function of distance from the Sun d, and R is the universal gas constant. In Fig. 8 (orange lines and right y axis) the sublimation lifetime of 1 nm sized dust particles made of carbon, silicate, and $Fe_{0.4}Mg_{0.6}O$ is shown again within the temperature range from 500 to 3000 K. As the vapour pressure of carbon is relatively low, the carbon nanodust has the longest sublimation lifetime. The oxides on the other hand have much shorter lifetimes. Astronomical silicate has slightly higher vapour pressure than $Fe_{0.4}Mg_{0.6}O$ because of its SiO_2 content.

As the vapour pressure is a very steep function of temperature, according to Eq. (8) the relationship is inversely translated to the sublimation lifetime. At temperatures below 1000 K the lifetimes of all different kinds of 1 nm dust are larger than 10^5 d. Nanodust with temperatures above 2500 K already have sublimation lifetimes below 10^{-5} d; these lifetimes are so short that the dust can be regarded as nonexistent.

The next step will be the direct comparison of sublimation and sputtering lifetimes for nanodust within the near-Sun environment.

4   Implications for nanodust near the Sun

In the earlier sections, it has been shown that sputtering and sublimation can be significant sinks for nanodust. The loss of nanodust due to solar wind sputtering increases with ion number density and ion mass (see Fig. 2). The effect of sublimation however is a steep function of dust temperature (see Sect. 3). For the comparison of sputtering and sublimation of nanodust, we have chosen the CME scenario. We find
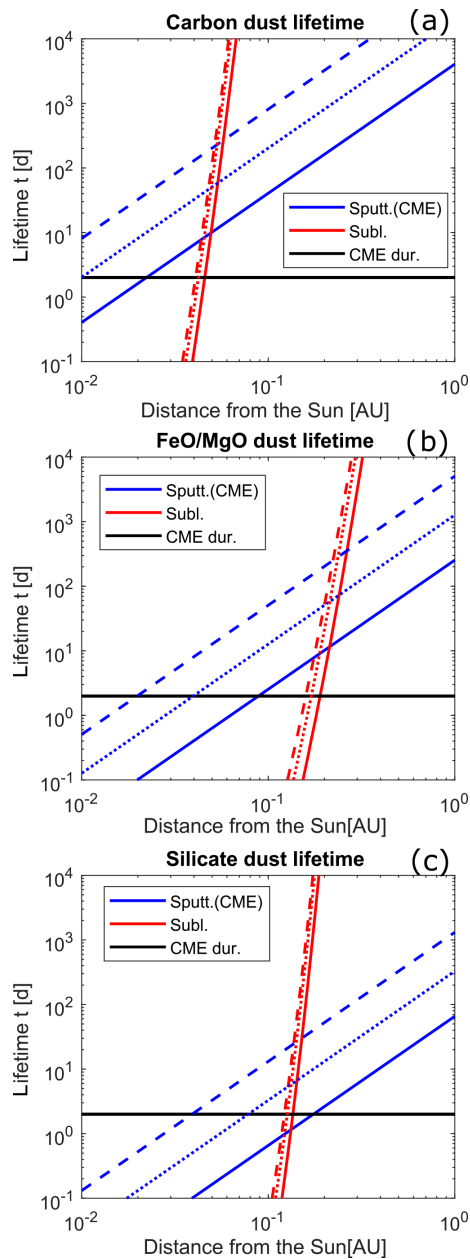
Figure 9. Comparison of sputtering and sublimation lifetimes of nanometre-sized dust near the Sun. Blue lines indicate sputtering lifetimes, red lines indicate sublimation lifetimes, line style indicates dust size (dotted – 5 nm, solid – 1 nm, dashed – 0.2 nm), and the 2 d duration of a typical CME is in black.

the shortest sputtering lifetimes for CME conditions, but the short duration of single CMEs has to be taken into account.

The comparison of the lifetimes is done in the small size limit of the dust population, i.e. the sizes 0.2, 1, and 5 nm. There is no experimental evidence for the existence of sub-nanometre dust. However, it will be hypothesized that these clusters of molecules exist. This assumption will help to better assess the importance of nanodust sputtering in this study.

Here, we compare the sputtering and sublimation lifetimes of the three different nanodust compositions, namely carbon, $Fe_{0.4}Mg_{0.6}O$, and silicate nanodust. Figure 9a shows the sputtering and sublimation lifetimes of carbon dust. All lifetimes are compared to a duration of 2 d, which is used as the upper limit for the duration of a CME. In the case of carbon, which is a rather sturdy material, the nanodust can survive in near proximity to the Sun. The sublimation of carbon nanodust within 2 d occurs at a distance of 0.03 AU from the Sun, which is because of carbon's comparably high evaporation temperature of 2600 K at low pressures (Whittaker, 1978). However, the sputtering lifetime of carbon is longer than its sublimation counterpart. The nanodust could withstand the sputtering of a CME to even shorter distances if it was not evaporated beforehand. When considering the duration of a CME, the sputtering and sublimation of only the smallest nanodust are comparable. In the case of carbon nanodust we state that during a typical CME sputtering is not a relevant destruction process within the inner heliosphere.

The lifetimes of $Fe_{0.4}Mg_{0.6}O$ dust for destruction by sublimation and sputtering are much shorter; see Fig. 9b. Due to its higher vapour pressure and temperature, the $Fe_{0.4}Mg_{0.6}O$ dust sublimates already at much larger distances from the Sun compared to the carbon dust. Just below 0.2 AU all $Fe_{0.4}Mg_{0.6}O$ nanodust is evaporated within the 2 d period. Despite the fact that $Fe_{0.4}Mg_{0.6}O$ material is much more vulnerable to sputtering (cf. Fig. 2) than carbon, a single CME cannot destroy nanodust by a single hit. A 1 nm $Fe_{0.4}Mg_{0.6}O$ dust grain would be completely sputtered by a CME if it reached 0.1 AU, but it will sublimate earlier due to its high temperature.

Regarding the sputtering and sublimation lifetime of silicate nanodust, we find a different situation compared to the aforementioned compositions. The actual lifetimes of silicate nanodust are shown in Fig. 9c. The sublimation lifetime of silicate nanodust equals the 2 d period at distances from the Sun of around 0.15 AU. The complete sputtering of the silicate nanodust during a CME impact occurs at solar distances of 0.2, 0.07, and 0.03 AU for the respective grain sizes 1, 5, and 20 nm. We can conclude here that a region void of silicate nanodust forms after the passage of a single CME. This region lies between 0.1 and 0.15 AU for the 1–3 nm dust; larger dust rather sublimates than being fully sputtered by a single CME. The existence of this sputtering region is due to the comparably low temperatures of silicate dust that lead to lower sublimation rates for the same distances as compared to the $Fe_{0.4}Mg_{0.6}O$ dust that is destroyed by sublimation.

4.1 Discussion

The results shown in Fig. 9a–c indicate a diverse influence of sublimation and sputtering on the nanodust environment near the Sun. The following remarks shall put the results into context for current and upcoming dust measurements near the Sun.

When dust particles approach the Sun, they heat up quickly and along with that the sublimation becomes the governing destruction process. One finding is that sublimation for nanodust is much less size dependent compared to the sputtering process. The derived sublimation lifetimes show that the governing parameters are the distance from the Sun, the resulting equilibrium temperature, and their composition.

The sputtering process on the other hand is much more size dependent but also shows distinct dependencies for dust composition and the increasingly harsh plasma environment near the Sun. Also, the type of plasma environment, i.e. slow or fast solar wind or CME impacts, present in the heliosphere plays an important role in the sputtering of nanodust. The importance of sputtering for the destruction of nanodust even at 1 AU can be seen in Fig. 5, where the dust sputtering lifetimes are well below the collisional and Poynting–Robertson lifetimes given by Grün et al. (1985). The change in the nanodust population through sputtering can result in different dust fluxes at 1 AU than expected so far. Additional measurements and dust flux modelling are needed to verify this finding.

As the sputtering and sublimation of nanodust are important destruction processes near the Sun, it can also be expected that the nanodust population will change its composition when approaching the Sun. While nanodust particles probably have a diverse composition at 1 AU and further away, only the most durable nanodust can survive near the Sun. Our calculation allows the assumption that the majority of nanodust in close proximity to the Sun contains large fractions of carbon in comparison to $Fe_{0.4}Mg_{0.6}O$ or silicate that are more likely sublimated or sputtered and not very abundant there. Quantitative statements on the abundance of different dust species also depend on their production rates near the Sun. Giving production rates for dust and nanodust made of different material is beyond the scope of this study.

Closer to the Sun, the nanodust population becomes even more variable under the influence of CME impacts. The sputtering lifetimes of nanodust under CME conditions are several orders of magnitude lower than for the solar wind conditions (Fig. 6). Void zones for silicate nanodust in the small size limit are identified after the passage of a mature CME impact. This finding would impact the nanodust population locally and during certain times, especially at solar maximum conditions when CMEs are frequent (up to 400 per month Lamy et al., 2019). This variability of the nanodust population might be quantified by impact measurements onboard Parker Solar Probe and Solar Orbiter, taking sputtering and also sublimation into account. Together with the onboard plasma and optical instruments, further constraints on the near-Sun nanodust population are possibly deduced.

The F-corona brightness at mid-infrared to visible wavelengths can be attributed to thermal emission from micronsized dust particles (Kimura and Mann, 1998). Recent WISPR observations on PSP (Howard et al., 2019) show that F-corona intensity leaves its linearity around 17 solar radii

(0.08 AU). These observations would support the existence of the predicted dust-free zones within the F corona (Lamy, 1974; Mann, 1992). In Sect. 2.2 we have identified sputtering by CME impacts as a possible destruction process also for µm dust. From Fig. 6, we find that a 10 µm dust particle can be fully destroyed within 3 years at a distance of 0.1 AU from the Sun when struck by multiple CMEs (assuming around 100 CMEs per month) and under constant exposure to the solar wind.

In the end, it has to be noted that the given lifetimes are only valid for dust on near-circular orbits. Dust affected by sublimation or sputtering is subject to a constant reduction of its size, which will result in alteration of its present orbit. The given results only represent a general description of these destruction processes. However, conclusions on the impact of sputtering and sublimation on individual dust grains along their orbits cannot be drawn and are not the subject of this work.

5 Conclusions

Interplanetary dust enters a harsh environment when approaching the proximity of our central star. Especially the small nanodust is prone to destruction through sputtering by the solar wind or sublimation near the Sun. Studies on dust destruction mechanisms near the Sun already showed that there are distinct regions dominated by sublimation and sputtering in the heliosphere (e.g. Mukai and Schwehm, 1981). This study has investigated dust sputtering during more extreme conditions of coronal mass ejection (CME) events. CME plasma in addition to its high number density contains a large fraction of heavy ions. We find that dust is sputtered most effectively in the CME case followed by sputtering within the slow solar wind. The weakest sputtering we find in the low-density plasma of the fast solar wind. However, the sputtering process is also very composition dependent. Carbon has been found to be more stable against sputtering than the silicate and $Fe_{0.4}Mg_{0.6}O$ composition. The case of nanodust has been studied in more detail for sputtering and sublimation during the passage of a single CME. Nanodust-free zones can occur after 2 d CMEs for silicate (0.1 to 0.15 AU), but not for $Fe_{0.4}Mg_{0.6}O$ and carbon.

The dust component near the Sun is in the process of being probed in unprecedented detail. While Parker Solar Probe is closing in on a proximity to the Sun of as close as 9 solar radii, Solar Orbiter will reach 0.3 AU but also observe the Sun outside the ecliptic plane. Both missions carry instruments to measure the local electric field (Bale et al., 2016; Maksimovic et al., 2007), which also enables the detection of dust impacts on the spacecraft. Taking into account sublimation and sputtering will be crucial to the modelling of the measured dust fluxes. This present work gives the needed insights and wants to encourage mindfulness of these processes when interpreting the satellite measurements. An ad-

ditional possibility of characterizing the composition of dust near the Sun is the detection of emission lines from sublimated dust atoms or ions. At 0.1 AU sublimation starts to be effective and might lead to layers of atomic species. Also, collisional dust destruction can be a source of ions which might be visible near the Sun (Mann and Czechowski, 2005). These ions might be detected optically from specific emission lines or using in situ mass spectrometric measurements onboard spacecraft.

The implementation of sputtering and sublimation as destruction mechanisms needs to be included in dust flux models, especially for the case of dust in the small size limit. Taking these processes into account is definitely important when considering the dust population near the Sun or other central stars. But also when considering dust trajectory modelling, the rough environment near stars leads to a shrinking of dust particles due to sublimation and sputtering. That leads to an increase in the often used charge to mass ratio of dust in these trajectory models for the small dust component. We expect that integrating the change in the dust size together with its full equation of motion will lead to new insights into the nanodust population near central stars. A recent study by Shestakova and Demchenko (2018) derived the orbital evolution of µm dust within the sublimation zone and included the dust size reduction due to sublimation. They find either elongated dust trajectories after partial sublimation or trajectories leading to complete sublimation after spiralling further into the evaporation zone of the Sun. A future study which also takes the sputtering of dust into account will find deeper insight into the fate of nanodust near the Sun and during the passage of a CME.

Variations in the F-corona intensity usually have been explained by the destruction of dust through sublimation or orbital changes (Lamy, 1974; Mann, 1992). The results of our work have shown that sputtering of micron-sized dust during the passage of multiple CMEs can play a role in the explanation of dust-free zones in the F corona.

Furthermore, we also expect that standard solar wind conditions can lead to significant sputtering in timescales which are shorter than the dynamical removal times of dust within intermediate distances from the Sun, i.e. 1 AU and further out.

Nevertheless, further laboratory as well as theoretical research is necessary to pinpoint sputtering yields for small dust grains of various composition. At the moment, experimental, theoretical, and modelling results of sputtering yields show a diverse picture where scientific consensus is missing.

Author contributions. CB carried out the calculations and wrote the initial manuscript. MM contributed the dust temperatures near the Sun. CB and IM conceived the idea of the work. All the authors contributed to the finalization of the manuscript.

References

Bale, S. D., Goetz, K., Harvey, P. R., Turin, P., Bonnell, J. W., Dudok de Wit, T., Ergun, R. E., MacDowall, R. J., Pulupa, M., Andre, M., Bolton, M., Bougeret, J.-L., Bowen, T. A., Burgess, D., Cattell, C. A., Chandran, B. D. G., Chaston, C. C., Chen, C. H. K., Choi, M. K., Connerney, J. E., Cranmer, S., Diaz-Aguado, M., Donakowski, W., Drake, J. F., Farrell, W. M., Fergeau, P., Fermin, J., Fischer, J., Fox, N., Glaser, D., Goldstein, M., Gordon, D., Hanson, E., Harris, S. E., Hayes, L. M., Hinze, J. J., Hollweg, J. V., Horbury, T. S., Howard, R. A., Hoxie, V., Jannet, G., Karlsson, M., Kasper, J. C., Kellogg, P. J., Kien, M., Klimchuk, J. A., Krasnoselskikh, V. V., Krucker, S., Lynch, J. J., Maksimovic, M., Malaspina, D. M., Marker, S., Martin, P., Martinez-Oliveros, J., McCauley, J., McComas, D. J., McDonald, T., Meyer-Vernet, N., Moncuquet, M., Monson, S. J., Mozer, F. S., Murphy, S. D., Odom, J., Oliverson, R., Olson, J., Parker, E. N., Pankow, D., Phan, T., Quataert, E., Quinn, T., Ruplin, S. W., Salem, C., Seitz, D., Sheppard, D. A., Siy, A., Stevens, K., Summers, D., Szabo, A., Timofeeva, M., Vaivads, A., Velli, M., Yehle, A., Werthimer, D., and Wygant, J. R.: The FIELDS In-

strument Suite for Solar Probe Plus, Space Sci. Rev., 204, 49–82, https://doi.org/10.1007/s11214-016-0244-5, 2016.

Barlow, M. J.: The destruction and growth of dust grains in interstellar space - I. Destruction by sputtering, Mon. Not. R. Astron. Soc., 183, 367–395, https://doi.org/10.1093/mnras/183.3.367, 1978.

Behrisch, R. and Eckstein, W.: Sputtering by particle bombardment: experiments and computer calculations from threshold to MeV energies, vol. 110, Springer Science & Business Media, 2007.

Czechowski, A. and Kleimann, J.: Nanodust dynamics during a coronal mass ejection, Ann. Geophys., 35, 1033–1049, https://doi.org/10.5194/angeo-35-1033-2017, 2017.

Czechowski, A. and Mann, I.: Formation and Acceleration of Nano Dust in the Inner Heliosphere, Astrophys. J., 714, 89, https://doi.org/10.1088/0004-637X/714/1/89, 2010.

Draine, B. T. and Salpeter, E. E.: Destruction mechanisms for interstellar dust, Astrophys. J., 231, 438–455, https://doi.org/10.1086/157206, 1979.

Duschl, W. J., Gail, H.-P., and Tscharnuter, W. M.: Destruction processes for dust in protoplanetary accretion disks., Astron. Astrophys., 312, 624–642, 1996.

Eckstein, W. and Preuss, R.: New fit formulae for the sputtering yield, Journal of Nuclear Materials, 320, 209–213, https://doi.org/10.1016/S0022-3115(03)00192-2, 2003.

Fegley Jr, B. and Cameron, A. G. W.: A vaporization model for iron/silicate fractionation in the Mercury protoplanet, Earth Planet. Sc. Lett., 82, 207–222, https://doi.org/10.1016/0012-821X(87)90196-8, 1987.

Fox, N., Velli, M., Bale, S., Decker, R., Driesman, A., Howard, R., Kasper, J., Kinnison, J., Kusterer, M., Lario, D., Lockwood, M., McComas, D., Raouafi, N., and Szabo, A.: The Solar Probe Plus Mission: Humanity's First Visit to Our Star, Space Sci. Rev., 204, 7–48, https://doi.org/10.1007/s11214-015-0211-6, 2016.

Greene, J. E.: Review Article: Tracing the recorded history of thin-film sputter deposition: From the 1800s to 2017, J. Vac. Sci. Technol. A, 35, 05C204, https://doi.org/10.1116/1.4998940, 2017.

Grün, E., Zook, H. A., Fechtig, H., and Giese, R. H.: Collisional balance of the meteoritic complex, Icarus, 62, 244–272, https://doi.org/10.1016/0019-1035(85)90121-6, 1985.

Hansen, C. J., Esposito, L., Stewart, A. I. F., Colwell, J., Hendrix, A., Pryor, W., Shemansky, D., and West, R.: Enceladus Water Vapor Plume, Science, 311, 1422–1425, https://doi.org/10.1126/science.1121254, 2006.

Hayderer, G., Cernusca, S., Schmid, M., Varga, P., Winter, H., Aumayr, F., Niemann, D., Hoffmann, V., Stolterfoht, N., Lemell, C., Wirtz, L., and Burgdörfer, J.: Kinetically Assisted Potential Sputtering of Insulators by Highly Charged Ions, Phys. Rev. Lett., 86, 3530–3533, https://doi.org/10.1103/PhysRevLett.86.3530, 2001.

Henning, T., Begemann, B., Mutschke, H., and Dorschner, J.: Optical properties of oxide dust grains., Astron. Astrophys., Supplement, 112, 143, http://articles.adsabs.harvard.edu/pdf/1995A%26AS..112..143H, 1995.

Howard, R. A., Vourlidas, A., Bothmer, V., Colaninno, R. C., DeForest, C. E., Gallagher, B., Hall, J. R., Hess, P., Higginso, A. K., Korendyke, C. M., Kouloumvakos, A., Lamy, P. L., Liewer, P. C., Linker, J., Linton, M., Penteado, P., Plunkett, S. P., Poirier, N., Raouafi, N. E., Rich, N., Rochus, P., Roulliard, A. P., Socker, D. G., Stenborg, G., Thernisien, A. F., and Viall, N. M.: Near-Sun observations of an F-corona decrease and K-corona fine structure, Nature, 576, 232–236, https://doi.org/10.1038/s41586-019-1807-x, 2019.

Järvi, T. T., Pakarinen, J. A., Kuronen, A., and Nordlund, K.: Enhanced sputtering from nanoparticles and thin films: Size effects, EPL (Europhysics Letters), 82, 26 002, https://doi.org/10.1209/0295-5075/82/26002, 2008.

Johnson, R. E., Famá, M., Liu, M., Baragiola, R. A., Sittler, E. C., and Smith, H. T.: Sputtering of ice grains and icy satellites in Saturn's inner magnetosphere, Planet. Space Sci., 56, 1238–1243, https://doi.org/10.1016/j.pss.2008.04.003, 2008.

Killen, R. M., Hurley, D. M., and Farrell, W. M.: The effect on the lunar exosphere of a coronal mass ejection passage, J. Geophys. Res.: Planets, 117, https://doi.org/10.1029/2011JE004011, 2012.

Kimura, H. and Mann, I.: Brightness of the solar F-corona, Earth Planets Space, 50, 493–499, https://doi.org/10.1186/BF03352140, 1998.

Lamy, P. L.: Interaction of interplanetary dust grains with the solar radiation field, Astron. Astrophys., 35, 197–207, http://adsabs.harvard.edu/full/1974A%26A....35..197L, 1974.

Lamy, P. L., Floyd, O., Boclet, B., Wjak, J., Gilardy, H., and Barlyaeva, T.: Coronal Mass Ejections over Solar Cycles 23 and 24, Space Sci. Rev., 215, 39, https://doi.org/10.1007/s11214-019-0605-y, 2019.

Leider, H. R., Krikorian, O. H., and Young, D. A.: Thermodynamic properties of carbon up to the critical point, Carbon, 11, 555–563, https://doi.org/https://doi.org/10.1016/0008-6223(73)90316-3, 1973.

Li, A. and Greenberg, J. M.: A unified model of interstellar dust., Astron. Astrophys., 323, 566–584, https://ui.adsabs.harvard.edu/abs/1997A%26A...323..566L/abstract, 1997.

Lide, D. R., ed.: Handbook of Chemistry and Physics, 84th Edition, chap. Section 6, Fluid Properties; Vapor Pressure, CRC Press, 2003.

Maksimovic, M., Zouganelis, I., Chaufray, J.-Y., Issautier, K., Scime, E. E., Littleton, J. E., Marsch, E., McComas, D. J., Salem, C., Lin, R. P., and Elliott, H.: Radial evolution of the electron distribution functions in the fast solar wind between 0.3 and 1.5 AU, J. Geophys. Res.: Space Physics, 110, https://doi.org/10.1029/2005JA011119, 2005.

Maksimovic, M., Bale, S. D., Vaivads, A., Krasnoselskikh, V., Chust, T., Balikhin, M., Goetz, K., Gough, P., Travnicek, P., Soucek, J., and Rucker, H.: A Radio And Plasma Wave Experiment For The Solar Orbiter Mission, in: Second Solar Orbiter Workshop, vol. 641 of ESA Special Publication, p. 38, 2007.

Mann, I.: The solar F-corona: calculations of the optical and infrared brightness of circumstellar dust., Astron. Astrophys, 261, 329–335, https://ui.adsabs.harvard.edu/abs/1992A&A...261.329M, 1992.

Mann, I. and Czechowski, A.: Dust Destruction and Ion Formation in the Inner Solar System, Astrophys. J. Lett., 621, L73–L76, https://doi.org/10.1086/429129, 2005.

Mann, I., Kimura, H., Biesecker, D. A., Tsurutani, B. T., Grün, E., McKibben, R. B., Liou, J.-C., MacQueen, R. M., Mukai, T., Guhathakurta, M., and Lamy, P.: Dust Near The Sun, Space Sci. Rev., 110, 269–305, https://doi.org/10.1023/B:SPAC.0000023440.82735.ba, 2004.

Mann, I., Nouzák, L., Vaverka, J., Antonsen, T., Fredriksen, Å., Issautier, K., Malaspina, D., Meyer-Vernet, N., Pavlů, J., Ster-

novsky, Z., Stude, J., Ye, S., and Zaslavsky, A.: Dust observations with antenna measurements and its prospects for observations with Parker Solar Probe and Solar Orbiter, Ann. Geophys, 37, 1121–1140, https://doi.org/10.5194/angeo-37-1121-2019, 2019.

McGrath, M., Johnson, R., and Lanzerotti, L.: Sputtering of sodium on the planet Mercury, Nature, 323, 694–696, https://doi.org/10.1038/323694a0, 1986.

Meyer-Vernet, N., Lecacheux, A., Kaiser, M. L., and Gurnett, D. A.: Detecting nanoparticles at radio frequencies: Jovian dust stream impacts on Cassini/RPWS, Geophys. Res. Let., 36, https://doi.org/10.1029/2008GL036752, 2009a.

Meyer-Vernet, N., Maksimovic, M., Czechowski, A., Mann, I., Zouganelis, I., Goetz, K., Kaiser, M. L., St. Cyr, O. C., Bougeret, J.-L., and Bale, S. D.: Dust Detection by the Wave Instrument on STEREO: Nanoparticles Picked up by the Solar Wind?, Sol. Phys., 256, 463–474, https://doi.org/10.1007/s11207-009-9349-2, 2009b.

Mukai, T. and Schwehm, G.: Interaction of grains with the solar energetic particles, Astron. Astrophys., 95, 373–382, http://adsabs.harvard.edu/full/1981A%26A....95..373Mr, 1981.

Müller, D., Marsden, R. G., St. Cyr, O. C., and Gilbert, H. R.: Solar Orbiter - Exploring the Sun–Heliosphere Connection, Sol. Phys., 285, 25–70, https://doi.org/10.1007/s11207-012-0085-7, 2013.

Myrvang, M.: Temperature and thermal emission of cosmic dust around the Sun, Vega and Fomalhaut, Master's thesis, UiT The Arctic University of Norway, https://hdl.handle.net/10037/13548, 2018.

Ragot, B. R. and Kahler, S. W.: Interactions of Dust Grains with Coronal Mass Ejections and Solar Cycle Variations of the F-Coronal Brightness, Astrophys. J., 594, 1049, https://doi.org/10.1086/377076, 2003.

Roth, J. and Möller, W.: Mechanism of enhanced sputtering of carbon at temperatures above 1200°C, Nucl. Instrum. Meth. B, 7-8, 788–792, https://doi.org/10.1016/0168-583X(85)90470-7, 1985.

Ruzic, D. N.: The effects of surface roughness characterized by fractal geometry on sputtering, Nucl. Instrum. Meth. B, 47, 118–125, https://doi.org/10.1016/0168-583X(90)90019-Q, 1990.

Schaefer, L. and Fegley, B.: A thermodynamic model of high temperature lava vaporization on Io, Icarus, 169, 216–241, https://doi.org/10.1016/j.icarus.2003.08.023, special Issue: Io after Galileo, 2004.

Schult, C., Stober, G., Keuer, D., and Singer, W.: Radar observations of the Maribo fireball over Juliusruh: revised trajectory and meteoroid mass estimation, Mon. Not. R. Astron. Soc., 450, 1460–1464, https://doi.org/10.1093/mnras/stv614, 2015.

Schwehm, G. H.: Temperaturverteilung und Dynamik interplanetarer Staubteilchen in der Nähe der Sonne, Ph.D. thesis, Ruhr-Universität Bochum, 1980.

Shestakova, L. I. and Demchenko, B. I.: Orbital Evolution of Dust Particles in the Sublimation Zone near the Sun, Sol. System Res., 52, 153–167, https://doi.org/10.1134/S0038094618010082, 2018.

Stamm, J., Czechowski, A., Mann, I., Baumann, C., and Myrvang, M.: Dust trajectory simulations around the Sun, Vega, and Fomalhaut, Astron. Astrophys., 626, A107, https://doi.org/10.1051/0004-6361/201834727, 2019.

Szalay, J. R., Pokorny, P., Bale, S. D., Christian, E. R., Goetz, K., Goodrich, K., Hill, M. E., Kuchner, M., Larsen, R., Malaspina, D., and et al.: The Near-Sun Dust Environment: Initial Observations from Parker Solar Probe, Astrophys. J. Supp. S., 246, 27, https://doi.org/10.3847/1538-4365/ab50c1, 2020.

Vorburger, A., Pfleger, M., Lindkvist, J., Holmström, M., Lammer, H., Lichtenegger, H. I. M., Galli, A., Rubin, M., and Wurz, P.: Three-Dimensional Modeling of Callisto's Surface Sputtered Exosphere Environment, J. Geophys. Res.: Space Physics, 124, 7157–7169, https://doi.org/10.1029/2019JA026610, 2019.

Whittaker, A. G.: Carbon: A New View of Its High-Temperature Behavior, Science, 200, 763–764, https://doi.org/10.1126/science.200.4343.763, 1978.

Wurz, P.: Erosion Processes Affecting Interplanetary Dust Grains, pp. 161–178, Springer Berlin Heidelberg, Berlin, Heidelberg, https://doi.org/10.1007/978-3-642-27543-2_8, 2012.

Wurz, P., Rohner, U., Whitby, J. A., Kolb, C., Lammer, H., Dobnikar, P., and Martín-Fernández, J. A.: The lunar exosphere: The sputtering contribution, Icarus, 191, 486–496, https://doi.org/10.1016/j.icarus.2007.04.034, 2007.

Wurz, P., Whitby, J. A., Rohner, U., Martín-Fernández, J. A., Lammer, H., and Kolb, C.: Self-consistent modelling of Mercury's exosphere by sputtering, micro-meteorite impact and photon-stimulated desorption, Planet. Space Sci., 58, 1599–1616, https://doi.org/10.1016/j.pss.2010.08.003, 2010.

Wurz, P., Rubin, M., Altwegg, K., Balsiger, H., Berthelier, J.-J., Bieler, A., Calmonte, U., De Keyser, J., Fiethe, B., Fuselier, S. A., Galli, A., Gasc, S., Gombosi, T. I., Jäckel, A., Le Roy, L., Mall, U. A., Rème, H., Tenishev, V., and Tzou, C.-Y.: Solar wind sputtering of dust on the surface of 67P/Churyumov-Gerasimenko, Astron. Astrophys., 583, A22, https://doi.org/10.1051/0004-6361/201525980, 2015.

Zaslavsky, A.: Floating potential perturbations due to micrometeoroid impacts: Theory and application to S/WAVES data, J. Geophys. Res.: Space Physics, 120, 855–867, https://doi.org/10.1002/2014JA020635, 2015.

Ziegler, J. F., Biersack, J. P., and Ziegler, M. D.: SRIM, the Stopping and Range of Ions in Matter, SRIM Company, 2008.